Progress In Electromagnetics Research Letters, Vol. 22, 119–128, 2011

SELECTIVE SUPPRESSION OF ELECTROMAGNETIC MODES IN A RECTANGULAR WAVEGUIDE BY USING DISTRIBUTED WALL LOSSES

C.-Q. Jiao

Beijing Key Laboratory of High Voltage and EMC
North China Electric Power University, Beijing 102206, China

Abstract—An over-mode metal rectangular waveguide is widely used in the generation, propagation, coupling, and transition of microwaves. When applied as the beam-wave interaction circuit of some high power microwave devices, a rectangular waveguide is expected to operate at a single electromagnetic mode. To do that, unwanted modes resulted from spurious oscillations should be suppressed. In this paper, a method of selective suppression of electromagnetic modes in rectangular waveguides by loading distributed losses in some special position of waveguide inner wall is presented. By using the method, the unwanted modes can be attenuated much larger relative to the operating mode. The presented method can be used to improve the stability of rectangular waveguide beam-wave interaction circuit.

1. INTRODUCTION

An over-mode metal rectangular waveguide is widely used in the generation, propagation, coupling, and transition of microwaves [1–4]. Almost applications require the rectangular waveguide to operate at a single-mode status. For some usual application, the status can be achieved by selecting appropriate waveguide dimensions and wave frequency to make only the lowest order mode (TE_{10}) not cut off.

However, for some special application, a single mode status is not so easy to be obtained. For example, when a rectangular waveguide is applied as the beam-wave interaction circuit of vacuum electron devices like the gyrotron, unwanted modes can be excited by spurious oscillations resulted from various beam-wave instabilities [5–13].

Received 31 January 2011, Accepted 11 March 2011, Scheduled 29 March 2011
Corresponding author: Chong-Qing Jiao (cqjiao@ncepu.edu.cn).

In order to suppress the unwanted modes, some technical measures have been presented. One of these measures is the distributed wall losses technique [14–17]. Distributed wall losses can be implemented by coating the inner wall of interaction circuit with finite conductivity material, which then can attenuate electromagnetic modes in the circuit, including both operating mode and unwanted modes. The attenuation for unwanted modes can effectively suppress their excitations. The attenuation for operating modes can reduce its amplification gain per unit length but the total gain may not be influenced because the total length of interaction circuit can be increased due to the improvement of interaction stability.

As is well known, the losses strength resulted from the lossy wall is proportional to the wall surface current density. Each of the electromagnetic modes has its own special current density distribution on the waveguide wall. Therefore, for a given mode, the losses strength is strongly dependent on where the lossy material loaded. Moreover, different modes take on different reaction to the change of lossy material's position. So, it is possible to selectively suppress electromagnetic modes in rectangular waveguides by loading lossy material in some special position. In this paper, the selective suppression properties of rectangular waveguide are investigated theoretically and some typical calculation results are presented. This paper is organized as follows. The characteristics of wall current distribution of rectangular waveguide are put up in Section 2. The analytic formula of propagation constants of electromagnetic modes in lossy rectangular waveguide is given in Section 3. Numerical results and discussions are made in Section 4, and this work is summarized in Section 5.

2. WALL CURRENT DISTRIBUTION IN A RECTANGULAR WAVEGUIDE

Since a gyrotron usually is operated at a TE mode, only TE mode is considered in the following study. The rectangular waveguide is shown in Fig. 1, with its inner dimensions given by a for the width and b for the height. The x, y and z axes are placed along the broad side, narrow side and the axis of the waveguide. The magnetic field components of the TE_{mn} mode in the rectangular waveguide with perfect conductor wall can be expresses as

$$H_z = H_{zm} \cos(k_x x) \cos(k_y y) \cos(\omega t - k_z z), \quad (1)$$

$$H_x = -\frac{k_z k_x}{k_c^2} H_{zm} \sin(k_x x) \cos(k_y y) \sin(\omega t - k_z z), \quad (2)$$

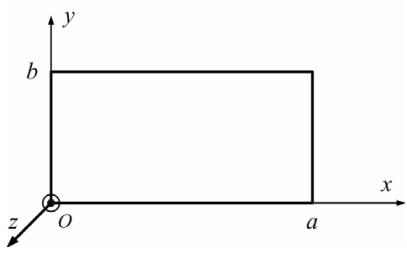

Figure 1. The cross section of a rectangular waveguide.

$$H_y = -\frac{k_z k_y}{k_c^2} H_{zm} \cos(k_x x) \sin(k_y y) \sin(\omega t - k_z z). \tag{3}$$

wherein, $k_x = \frac{m\pi}{a}$, $k_y = \frac{n\pi}{b}$, $k_{mn} = \sqrt{k_x^2 + k_y^2}$, $k_z = \sqrt{k^2 - k_{mn}^2}$, $k = \omega/c$, and H_{zm} is the amplitude of the axial magnetic field H_z.

The surface current density on the inner wall can be obtained by

$$\vec{J} = \vec{e}_n \times \vec{H}, \tag{4}$$

wherein, $\vec{e}_n$ is the unit vector normal to the waveguide wall. Substituting Eqs. (1)–(3) into Eq. (4), we can find that the root-mean-square value of the current density is

$$J = \frac{1}{\sqrt{2}} H_{zm} \left[\cos^2(k_y y) \left(1 - \left(\frac{k_z k_y}{k_{mn}^2} \right)^2 \right) + \left(\frac{k_z k_y}{k_{mn}^2} \right)^2 \right]^{1/2}, \tag{5}$$

at the $x = 0$ and $x = a$ walls and

$$J = \frac{1}{\sqrt{2}} H_{zm} \left[\cos^2(k_x x) \left(1 - \left(\frac{k_z k_x}{k_{mn}^2} \right)^2 \right) + \left(\frac{k_z k_x}{k_{mn}^2} \right)^2 \right]^{1/2}, \tag{6}$$

at the $y = 0$ and $y = b$ walls.

From Eqs. (5) and (6), it can be found that, the maximum current density happens at the positions with $\cos^2(k_y y) = 1$ for the $x = 0$ and $x = a$ walls and $\cos^2(k_x x) = 1$ for the $y = 0$ and $y = a$ walls.

3. ANALYTIC FORMULA OF PROPAGATION CONSTANT

The propagation of the electromagnetic wave along a lossy waveguide abides the $e^{j\omega t \gamma z}$ and the propagation constant γ can be written as

$$\gamma = \alpha + j\beta \tag{7}$$

where α and β are, respectively, the attenuation constant and phase constant.

Two kinds of approximate analytic model can be used to derive the propagation constant. One is the power loss model [18, 19]. This model considers the attenuation constant as the ratio of the power loss on per unit length to the power transmitted in the waveguide. The transmitted power is approximated by that transmitted in a corresponding waveguide with perfect conductor wall. A wave can not propagate in a perfect waveguide if its frequency is below cutoff. So, the attenuation constant will be close to infinite and not feasible for frequencies close to and below cutoff. The second is the so called boundary impedance perturbation model [19–23]. This model can be used into the frequency range close to and below cutoff and the effect of wall loss on the phase constant can also be considered. Moreover, it can be proved that, the results from the two models are in good agreement when wave frequency is a little larger than cutoff.

According to the boundary impedance perturbation method, the propagation constant γ_{mn} of the TE_{mn} mode in a lossy waveguide with finite conductivity wall can be calculated using the following expression [19, 21]

$$\gamma_{mn}^2 = \gamma_0^2 - \frac{1-i}{2} \frac{\oint_l \delta \left[k_{mn}^4 \left|\phi_0\right|^2 + \gamma_0^2 \left| \frac{\partial \phi_0}{\partial \hat{l}} \right|^2 \right] \mathrm{d}l}{k_{mn}^2 \iint_S \left|\phi_0\right|^2 \mathrm{d}S} \tag{8}$$

wherein, $\gamma_0 = jk_z$, S denotes the cross section of waveguide, and l is the boundary curve of S, δ is the skin depth of the waveguide wall, and ϕ_0 represents the transverse distribution of axial magnetic field H_z. For the rectangular waveguide,

$$\phi_0 = \cos\left(k_x x\right) \cos\left(k_y y\right) \tag{9}$$

For example, when wall losses is coated around the center of the two broad sides as shown in Fig. 2, the propagation constant can be written as

$$\gamma_{mn}^2 = \gamma_0^2 - \frac{1-i}{2} L \chi_m \chi_n \delta \frac{\left(k_{mn}^4 - \gamma_0^2 k_x^2\right) + (-1)^m \left(k_{mn}^4 + \gamma_0^2 k_x^2\right) \frac{\sin k_x L}{k_x L}}{k_{mn}^2 ab}. \tag{10}$$

where, χ_m equals 1 if $m = 0$ or 2 if $m \neq 0$, χ_n equals 1 if $n = 0$ or 2 if $n \neq 0$, and $\sin(k_x L)/(k_x L) = 1$ for TE_{0n} modes. For theses modes, $m = 0$ and so $k_x = 0$.

In [21, 24], the validity of Eq. (8) had been confirmed by comparison with results obtained using high-frequency structure simulator (HFSS).

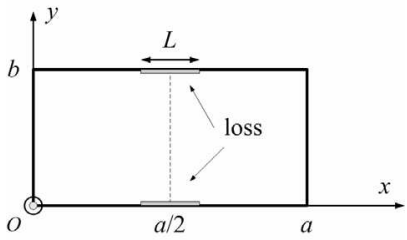

Figure 2. Rectangular waveguide with wall losses distributed around the center of the broad side.

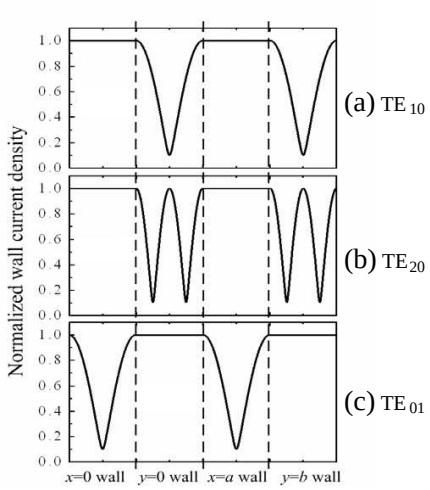

Figure 3. Normalized wall current density distribution along the cross section of the rectangular waveguide with $a = 2b$ and $k_z = 0.1k_{mn}$, (a) TE_{10} mode, (b) TE_{20} mode, (c) TE_{01} mode.

4. RESULTS AND DISCUSSIONS

Three modes, TE_{10}, TE_{20}, and TE_{01} are considered in the following study. Also, the length of the broad side is assumed to be 2 times of the length of the narrow side ($a = 2b$). So, the TE_{20} and TE_{01} modes are degenerate. In addition, the TE_{10} mode is assumed to be the operating mode and the other two modes are the unwanted modes. According the current distribution presented in Section 2, Fig. 3 plots the normalized wall current density distribution along the cross section of the rectangular waveguide for the three modes. It should be noted that, in Fig. 3, the horizontal coordinates are divided into four segments by the three vertical dashed lines, corresponding

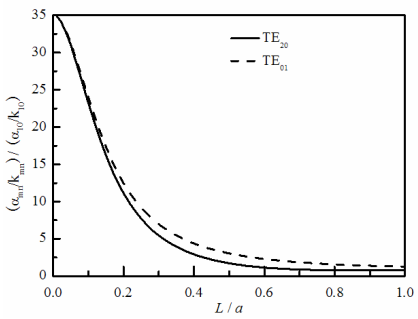

Figure 4. The ratio of the attenuation constants of the TE_{20} and TE_{01} modes to that of the TE_{10} mode as a function of the length of the lossy section for $f = 1.01 f_c$ and $\rho = 10^4 \rho_{cu}$.

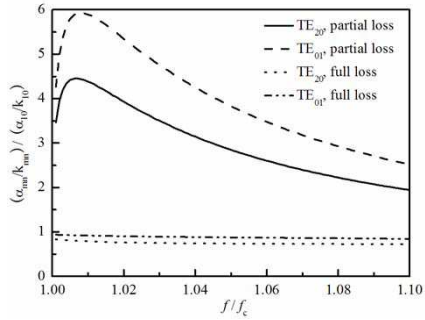

Figure 5. The ratio of the attenuation constants of the TE_{20} and TE_{01}modes to that of the TE_{10} mode as a function of the wave frequency for $L = a/3$ and $\rho = 10^4 \rho_{cu}$.

to the four walls of the waveguide. The horizontal coordinate variable is y for the $x = 0$ and $x = a$ walls, and x for the $y = 0$ and $y = b$ walls. It is easy to find that, at the position of $x = a/2$, the current density reaches its minimum for the TE_{10} mode and its maximum for the other two modes as shown in. So, wall losses configuration shown in Fig. 2 can be used to suppress the two unwanted modes.

Figure 4 plots the ratios of the normalized attenuation constants of the TE_{20} and TE_{01} modes to that of the TE_{10} mode as a function of the length of the lossy section. Wherein, α_{mn} and β_{mn} denotes the real and imaginary parts of γ_{mn}, respectively. The normalized attenuation constant is defined as the ratio of the attenuation constant α_{mn} to the cutoff wavenumber k_{mn}. The coated lossy material is assumed to have a resistivity $\rho = 10^4 \rho_{cu}$. $\rho_{cu} = 1.72 \times 10^{-8}\,\Omega \cdot \mathrm{m}$ is the resistivity of copper. For each mode, its wave frequency f is assumed to be 1.01 times of its cutoff frequency f_c.

As expected, the ratios decrease rapidly with the increment of the lossy section length L. Optimum suppression effect for the two unwanted modes can be achieved only when the lossy section is very short.

Figure 5 displays the ratios of the normalized attenuation constants of the TE_{20} and TE_{01} modes to that of the TE_{10} mode as a function of the wave frequency for $L = a/3$ and $\rho = 10^4 \rho_{cu}$. The ratios related to the case that the whole waveguide wall is coated with lossy material are also plotted for comparison and the corresponding curves are denoted with "full loss". We can see that, the ratios in the case

of "partial loss" are much larger than those in the case of "full loss". Optimum suppression effect can be achieved when the wave frequency is approximately equal to 1.01 cutoff frequency. The ratios in the case of "partial loss" will shift close to those in the case of "full loss" when the wave frequency is very larger than the cutoff frequency.

Figure 6 shows the ratios of the normalized attenuation constants of the TE_{20} and TE_{01} modes to that of the TE_{10} mode as a function of the resistivity for $L = a/3$ and $f = 1.01f_c$. For the case of "partial loss", the ratios keep unchanged when the resistivity is smaller than $10^3\rho_{cu}$ and begin to reduce slowly with further increase of the resistivity. Moreover, for the two degenerate modes, the attenuation of the TE_{01} mode is always larger than that of the TE_{20} mode, according to Figs. 4–6.

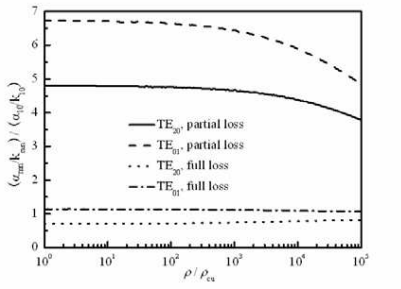

Figure 6. The ratio of the attenuation constants of the TE_{20} and TE_{01} modes to that of the TE_{10} mode as a function of the wall resistivity for $L = a/3$ and $f = 1.01f_c$.

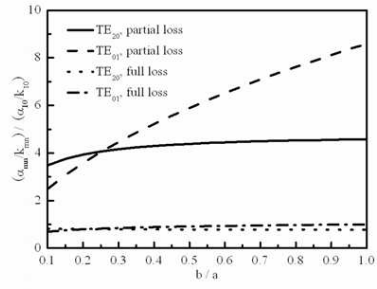

Figure 7. The ratio of the attenuation constants of the TE_{20} and TE_{01} modes to that of the TE_{10} mode as a function of b/a for $L = a/3$, $f = 1.01f_c$, and $\rho = 10^4\rho_{cu}$.

Figure 7 illuminates the ratio of the attenuation constants of the TE_{20} and TE_{01} modes to that of the TE_{10} mode as a function of b/a for $L = a/3$, $f = 1.01f_c$, and $\rho = 10^4\rho_{cu}$. The ratios corresponding to "full loss" still approximately keep fixed despite b/a changing within a wide range from 0.1 to 1. For the case of "partial loss", with the increment of b/a, the curve related to the TE_{20} mode increases slowly but that related to the TE_{01} mode does rapidly. The underlying reason is that, with the increment of b, the cutoff frequency of the TE_{20} mode keeps unchanged but that of the TE_{01} mode reduces. As a resulted, the normalized attenuation constant of the TE_{01} mode increases with the increment of b.

In the following, the TE_{20} mode is assumed to be the operating mode and the TE_{10} and TE_{01} modes are the unwanted modes. Wall

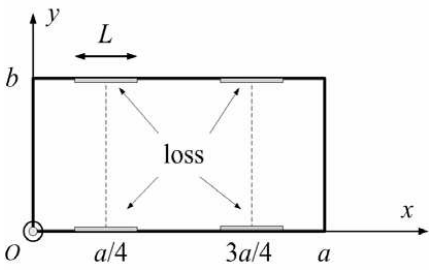

Figure 8. Rectangular waveguide with wall losses distributed around the quarter and three quarters of the broad side.

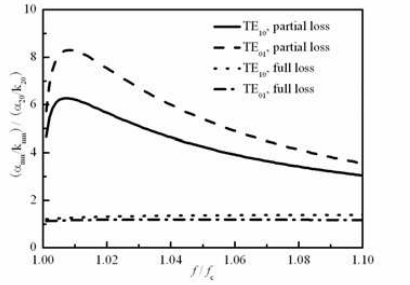

Figure 9. The ratio of the attenuation constants of the TE_{10} and TE_{01} modes to that of the TE_{20} mode as a function of the wave frequency for $L = a/6$ and $\rho = 10^4\rho_{cu}$.

losses configuration shown in Fig. 8 can be employed to suppress the two unwanted modes. Fig. 9 plots the ratios of the normalized attenuation constants of the TE_{10} and TE_{01} modes to that of the TE_{20} mode as a function of the wave frequency for $L = a/6$ and $\rho = 10^4\rho_{cu}$. From Fig. 9, it is also easy to find the effectiveness of this configuration. Similarly, the optimum suppression happens at $f = 1.01f_c$.

5. CONCLUSION

The idea of to selectively suppress electromagnetic modes in rectangular waveguide by using distributed losses is presented and investigated theoretically. Numerical results for three typical modes, including the TE_{10}, TE_{20}, and TE_{01} are given in detail. The effect of the wave frequency, the wall resistivity, and the lossy section length are analyzed. When the TE_{10} mode is the operating mode, the lossy material may be coated around the center of the broad side of the rectangular waveguide, and when the TE_{20} mode is the operating mode, the lossy material could be coated around the quarter and three quarters of the broad side.

ACKNOWLEDGMENT

This work was supported by "the Fundamental Research Funds for the Central Universities in China" (Grant No. 10MG01 and No. 09TG01).

REFERENCES

1. Soekmadji, H., S. Liao, and R. J. Vernon, "Experiment and simulation on TE_{10} cut-off reflection phase in gentle rectangular downtapers," *Progress In Electromagnetics Research Letters*, Vol. 12, 79–85, 2009.
2. Rothwell, E. J., A. K. Temme, and B. R. Crowgey, "Pulse reflection from a dielectric discontinuity in a rectangular waveguide," *Progress In Electromagnetics Research*, Vol. 97, 11–25, 2009.
3. Hussain, A. and Q. A. Naqvi, "Fractional rectangular impedance waveguide," *Progress In Electromagnetics Research*, Vol. 96, 101–116, 2009.
4. Hammou, D., E. Moldovan, and S. O. Tatu, "V-band microstrip to standard rectangular waveguide transition using a substrate interated waveguide (SIW)," *Journal of Electromagnetic Waves and Applications*, Vol. 23, No. 2–3, 221–230, 2009.
5. Zhao, D., Y. G. Ding, Y. Wang, and C. J. Ruan, "Linear analysis of a rectangular waveguide cyclotron maser with a sheet electron beam," *Phys. Plasmas*, Vol. 17, No. 11, 113110, 2010.
6. Mineo, M., A. Di Carlo, and C. Paoloni, "Analytic design method for corrugated rectangular waveguide SWS THz vacuum tubes," *Journal of Electromagnetic Waves and Applications*, Vol. 24, No. 17–18, 2479–2494, 2010.
7. Radack, D. J., K. Ramaswamy, W. W. Destler, and J. Rodgers, "A fundamental mode, high power, large-orbit gyrotron using a rectangular interaction region," *J. Appl. Phys.*, Vol. 73, No. 12, 8139–8145, 1993.
8. Lau, Y. Y. and L. R. Barnett, "A note on gyrotron traveling wave amplifiers using rectangular waveguides," *IEEE Trans. Electron. Devices*, Vol. 30, No. 8, 908–912, 1983.
9. Ferendeci, A. M. and C. C. Han, "Linear analysis of an axially grooved rectangular gyrotron for harmonic operation," *Int. J. Infrared Millim. Waves*, Vol. 6, No. 12, 1267–1283, 1985.
10. Soekmadji, H., S. L. Liao, and R. J. Vernon, "Trapped mode phenomena in a weakly overmoded waveguiding structure of rectangular cross section," *Journal of Electromagnetic Waves and Applications*, Vol. 22, No. 1, 143–157, 2008.
11. Kumar, N., U. Singh, A. Kumar, H. Khatun, T. P. Singh, and A. K. Sinha, "Design of 35 GHz gyrotron for material processing applications," *Progress In Electromagnetics Research B*, Vol. 27, 273–288, 2011.

12. Jain, R. and M. V. Kartikeyan, "Design of a 60 GHz, 100 kW cw gyrotron for plasma diagnostics: Gds-V.01 simulations," *Progress In Electromagnetics Research B*, Vol. 22, 379–399, 2010.
13. Malek, F., J. Lucas, and Y. Huang, "The experimental result of a low power x-band free electron maser by electron pre-bunching," *Progress In Electromagnetics Research*, Vol. 101, 43–62, 2010.
14. Chu, K. R., H. Y. Chen, C. L. Hung, et al., "Theory and experiment of ultrahigh gain gyrotron travelingwave amplifier," *IEEE Trans. Plasma. Sci.*, Vol. 27, No. 2, 391–404, 1999.
15. Jiao, C. Q. and J. R. Luo, "Study on the suppression of gyro-BWO by distributed wall losses," *J. Infrared. Milli. Terahz. Waves*, Vol. 30, No. 9, 924–930, 2009.
16. Pao, K. F., C. T. Fan, T. H. Chang, et al., "Selective suppression of high order axial modes of the gyrotron backward-wave oscillator," *Physics of Plasmas*, Vol. 14, No. 9, 093301, 2007.
17. Song, H. H., D. B. McDermott, Y. Hirata, et al., "Theory and experiment of a 94 GHz gyrotron traveling-wave amplifier," *Phys. Plasmas*, Vol. 11, No. 5, 2935–2941, 2004.
18. Zhang, K. Q. and D. J. Li, *Electromagnetic Theory for Microwaves and Optoelectronics*, Springer, New York, 1998.
19. Jackson, J. D., *Classical Electrodynamics*, 2nd edition, Wiley, New York, 1975.
20. Collin, R. E., *Field Theory of Guided Waves*, McGraw-Hill, New York, 1960.
21. Hung, C. L. and Y. S. Yeh, "The propagation constants of higher-order modes in coaxial waveguides with finite conductivity," *Int. J. Infrared. Mill. Waves*, Vol. 26, No. 1, 29–39, 2005.
22. Luo, J. R. and C. Q. Jiao, "Effect of the lossy layer thickness of metal cylindrical waveguide wall on the propagation constant of electromagnetic modes," *Appl. Phys. Lett.*, Vol. 88, No. 6, 061115, 2006.
23. Jiao, C. Q., N. Zheng, and J. R. Luo, "A comparison of the attenuation of high-order mode in coaxial waveguide due to inner and outer conductor losses," *J. Infrared. Milli. Terahz. Waves*, Vol. 31, No. 7, 858–865, 2010.
24. Yan, S., B. K. Huang, W. S. Jiang, and Y. S. Jiang, "Calculation of the propagation constants in waveguides with imperfect conductor by the perturbed boundary condition method," *Journal of Microwaves*, Vol. 26, No. 2, 35–38, 2010 (in Chinese).